Spectroscopic and crystal-field analysis of new Yb-doped laser materials

2001 J. Phys.: Condens. Matter 13 5427

(http://iopscience.iop.org/0953-8984/13/23/303)

INSTITUTE OF PHYSICS PUBLISHING JOURNAL OF PHYSICS: CONDENSED MATTER

J. Phys.: Condens. Matter **13** (2001) 5427–5447 www.iop.org/Journals/cm PII: S0953-8984(01)22027-X

Spectroscopic and crystal-field analysis of new Yb-doped laser materials

Paul-Henri Haumesser, Romain Gaumé, Bruno Viana[1], Elisabeth Antic-Fidancev and Daniel Vivien

Laboratoire de Chimie Appliquée de l'Etat Solide UMR 75 74, ENSCP, 11 rue Pierre et Marie Curie, 75231 Paris Cédex 05, France

E-mail: viana@ext.jussieu.fr (B Viana)

Received 15 February 2001

Abstract

Crystal-field effects are very important as far as laser performances of Yb-doped materials are concerned. In order to simplify the interpretation of low-temperature spectra, two tools derived from a careful examination of crystal-field interaction are presented. Both approaches are successfully applied in the case of new Yb-doped materials, namely $Ca_3Y_2(BO_3)_4$ (CYB), $Ca_3Gd_2(BO_3)_4$ (CaGB), $Sr_3Y(BO_3)_3$ (SrYBO), $Ba_3Lu(BO_3)_3$ (BLuB), Y_2SiO_5 (YSO), $Ca_2Al_2SiO_7$ (CAS) and $SrY_4(SiO_4)_3O$ (SYS). The $^2F_{7/2}$ splitting is particularly large in these materials and favourable to a quasi-three-level laser operating scheme. Calculations performed using the point charge electrostatic model for these compounds and using a consistent set of effective atomic charges confirm the experimental results. This should permit to use this model in a predictive approach.

1. Introduction

Yb-based laser systems for 1 μm emission have aroused much interest since the development of laser diodes adapted to the pumping of such lasers around 980 nm. From the spectroscopic point of view, ytterbium exhibits several advantages in comparison with neodymium. Due to the presence of only two electronic $^2F_{7/2}$ and $^2F_{5/2}$ manifolds, the Yb doping level can be very high, leading to a miniaturization of the devices without the problems (luminescence quenching due to the cross-relaxation process, excited-state absorption etc) encountered for the Nd-based laser systems [1].

However, a main drawback of ytterbium lasers is their quasi-three-level operating scheme, as the fundamental and terminal laser levels belong to the same manifold. Owing to this particular energy-level configuration, the spectroscopic characteristics and laser properties of ytterbium are particularly host dependent [2]. This arises from the sensitivity of the energy-level distribution to the crystal-field interaction. For instance, the $^2F_{7/2}$ manifold overall

[1] Author to whom any correspondence should be addressed.

0953-8984/01/235427+21$30.00

splitting is only of 492 cm^{-1} in $CaWO_4$ [3], whereas it reaches 1190 cm^{-1} in $Sr_5(PO_4)_3F$ (SFAP) [4], which is one of the highest known values. In order to limit thermal population of the terminal laser level, a ground-state splitting as large as possible is desirable. This implies that the crystal-field interaction experienced by the Yb^{3+} ions has to be maximal.

Unfortunately, no global survey of crystal-field effects in various Yb-doped hosts has been carried out until now, mainly due to the lack of data. The reason for this is twofold. The first explanation is related to the very simple electronic structure of Yb^{3+}: with only seven Stark levels distributed in the two manifolds, it is impossible to unequivocally derive from experimental data a phenomenological crystal-field potential described, according to the site symmetry, by up to 27 parameters. All available crystal-field descriptions concern thus hosts that have been studied with several lanthanide doping ions, the result being extrapolated to ytterbium [5]. The second reason for the lack of crystal-field data is the difficulty of deriving unambiguously the energy-level diagram from the low-temperature absorption and emission spectra. This is mainly due to the strong interaction of Yb^{3+} ions with the lattice vibrations [6]. These effects can give rise to strong vibronic sidebands [7] or to the deformation or splitting of electronic lines in the case of resonant coupling [8], which significantly complicates the low-temperature spectra.

In that context, this paper has three purposes. The first part will be devoted to an overview of energy-level and crystal-field data in the literature concerning Yb-doped oxides. From this study, two useful tools will be derived to help in determining energy-level diagrams of ytterbium from low-temperature spectra. In a second part, those tools will be used in the case of new Yb-doped materials. These compounds are the Y_2SiO_5 (YSO), $Ca_2Al_2SiO_7$ (CAS) and $SrY_4(SiO_4)_3O$ (SYS) silicates and the $Ca_3Y_2(BO_3)_4$ (CYB), $Ca_3Gd_2(BO_3)_4$ (CaGB), $Sr_3Y(BO_3)_3$ (SrYBO) and $Ba_3Lu(BO_3)_3$ (BLuB) double borates. Finally, we will propose a predictive tool based on the point charge electrostatic crystal-field model that should allow estimation of the crystal-field characteristics in a given host from structural data. We will demonstrate that such a model can be successfully used to predict at least the overall splitting of the Yb^{3+} manifolds in various hosts.

2. Crystal-field effects on Yb^{3+} energy-level distributions

This survey is based on the collection of Yb^{3+} energy-level distributions in various hosts described in the literature. An as exhaustive as possible study of the available data produced only a few relevant references. Among them, the most complete is the global survey carried out by Morrison and Leavitt on crystal-field and energy-level determination in various hosts for all the lanthanide ions [3]. Other useful contributions give the ytterbium energy-level distributions in $YAl_3(BO_3)_4$ (YAB) [9], $Ca_4GdO(BO_3)_3$ (GdCOB) [7] and in $KGd(WO_4)_2$ (KGW) and $KY(WO_4)_2$ (KYW) [10]. Crystal-field interaction analysis relating to Yb^{3+} is reported for YPO_4 and $LuPO_4$ [11], $Ca_5(PO_4)_3F$ (CFAP) [12] and Y_2O_3 [13]. Recent works have been devoted to the determination of electronic levels of ytterbium in the Y_2O_3, Sc_2O_3 and Lu_2O_3 sesquioxides [14] and $CsCdBr_3$ and $Cs_3Yb_2Br_9$ materials [15].

2.1. The effect on the spin–orbit splitting: the 'barycentres plot'

The separation between the $^2F_{7/2}$ (ground-state) and $^2F_{5/2}$ (excited-state) manifolds results from the spin–orbit interaction. For an ytterbium ion embedded in a host lattice, two distinct effects could alter this energy separation. The first one is a modification of the spin–orbit coupling constant ζ. However theoretically predicted, this variation is very weak for lanthanide ions [16]. The second possible effect is the J-mixing, which corresponds to the mixing by the

crystal field of states belonging to the $^2F_{7/2}$ and $^2F_{5/2}$ levels. This second-order interaction should increase the energy separation between the two manifolds. In the case of ytterbium, this energy difference (about 10 200 cm^{-1}) is large enough to neglect the J-mixing to a good approximation.

Hence, it is reasonable to consider that the energy separation between Yb^{3+} ground and excited states is constant whatever the host, and equal to the spin–orbit splitting measured for the free ion. More precisely, when taking the lowest Stark level as the origin of energies and plotting the $^2F_{5/2}$ manifold energy barycentre versus the $^2F_{7/2}$ one, the representative points should align on a straight line whose slope is equal to one [17]. In figure 1, we present this plot for several hosts for which reliable data are available (see table 1). As expected, data obtained from the literature are aligned on the constant-energy-separation line with an exception concerning the CFAP and SFAP matrices, for which vibronic lines may have been assigned to electronic transitions. One can also notice that the data are also in good agreement with results for materials such as $CsCdBr_3$ presenting mainly Yb–Yb pairs. This 'barycentres plot' is a useful tool for deriving energy-level distributions from low-temperature spectroscopic data, as will be shown below.

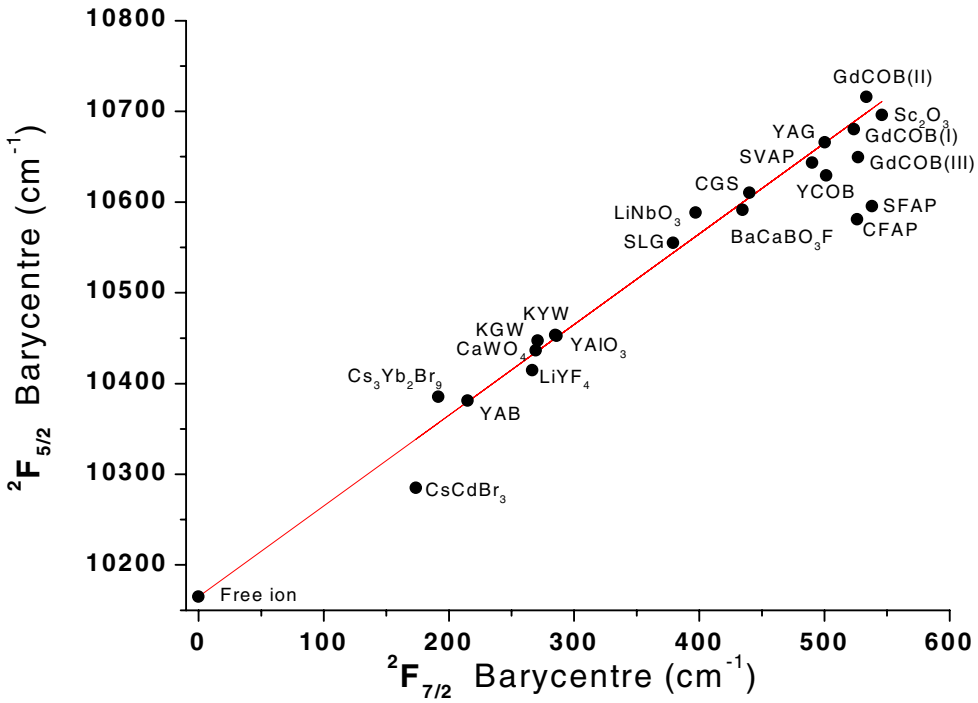

Figure 1. A barycentres plot for various Yb-doped materials.

2.2. *Crystal-field strength and Yb^{3+} manifold splitting*

A second useful concept is the crystal-field strength, introduced by F Auzel and O L Malta in the early 1980s [18]. They defined a scalar parameter calculated from the crystal-field

Table 1. Energy levels of ytterbium in various hosts.

Host	$^2F_{7/2}$ (cm^{-1})				$^2F_{5/2}$ (cm^{-1})			Reference
$Ca_2Ga_2SiO_7$ (CGS)	0	300	490	970	10250	10570	11010	[27]
$SrLaGa_3O_7$ (SLG)	0	220	386	910	10190	10450	11025	[27]
$Ca_4GdO(BO_3)_3$ (GdCOB) (site I, Gd)	0	423	668	1003	10246	10706	11089	[7]
GdCOB (site II, Ca)	0	437	694	1003	10261	10737	11150	[7]
GdCOB (site III, Ca)	0	417	688	1003	10240	10682	11026	[7]
$Ca_4YO(BO_3)_3$ (YCOB)	0	427	556	1023	10242	10537	11109	[28]
Sc_2O_3	0	474	634	1076	10250	10640	11198	[32]
$Ca_5(PO_4)_3F$ (CFAP)	0	409	597	1099	10178	10496	11069	[2]
$Sr_5(PO_4)_3F$ (SFAP)	0	362	618	1190	10150	10512	11108	[29]
$Sr_5(VO_4)_3F$ (SVAP)	0	321	562	1078	10141	10740	11050	[33]
$Y_3Al_5O_{12}$ (YAG)	0	584	635	783	10328	10752	10917	[30]
$BaCaBO_3F$ (BCBF)	0	303	533	902	10204	10570	11000	[34]
$LiNbO_3$	0	352	448	788	10204	10471	11090	[35]
$KGd(WO_4)_2$ (KGW)	0	163	385	535	10188	10471	10682	[10]
$KY(WO_4)_2$ (KYW)	0	169	407	568	10187	10476	10695	[10]
$CaWO_4$	0	220	366	492	10278	10366	10665	[3]
$YAlO_3$	0	209	341	590	10220	10410	10730	[3]
$LiYF_4$	0	216	371	479	10288	10409	10547	[3]
$YAl_3(BO_3)_4$ (YAB)	0	94	185	581	10194	10277	10672	[31]
$CsCdBr_3$	0	144	201	421	10277	10301	10578	[15]
$Cs_3Yb_2Br_9$	0	114	140	441	10119	10146	10590	[15]

parameters B_{kq} to evaluate the effect of crystal-field interaction on a $^{2S+1}L_J$ level, as follows:

$$N_J = \left[\sum_{\substack{k=2,4,6 \\ k \leqslant 2J}} \sum_{q=-k}^{k} (B_{kq})^2 \frac{4\pi}{2k+1} \right]^{1/2}. \tag{1}$$

A major point of interest as regards this parameter is the fact that it can be related to the crystal-field splitting of the $^{2S+1}L_J$ level through

$$\Delta E_J = \left(\frac{3g_a^2}{g(g_a+2)(g_a+1)\pi} \right)^{1/2} \left| \prod_{k=2,4,6} |\langle 3||C_k||3\rangle \langle LSJ||U_k||LSJ\rangle| \right|^{1/3} N_J \tag{2}$$

where g_a is the degeneracy lifted by the crystal field and g is the total degeneracy of the $^{2S+1}L_J$ manifold. Hence, the splitting of a given spectroscopic level is proportional to the crystal-field strength. Such a behaviour was demonstrated in the case of Nd^{3+} for the $^4I_{9/2}$ manifold [18]:

$$\Delta E(^4I_{9/2}) = 0.147N(^4I_{9/2}). \tag{3}$$

In a recent work [19], F Auzel extended this approach to the Yb^{3+} $^2F_{7/2}$ ground state, using equation (2), which led to the following relation:

$$\Delta E(^2F_{7/2}) = 0.246N(^2F_{7/2}). \tag{4}$$

A plot of the $^2F_{7/2}$ (Yb^{3+}) overall spitting versus crystal-field strength is presented in figure 2(c) for several Yb-doped materials for which reliable crystal-field data are available. The straight line of equation (4) is represented as well. It appears that the experimental points are aligned, but there is some mismatch with the theoretical line. This can be understood, as the constant of proportionality between $\Delta E(^2F_{7/2})$ and $N(^2F_{7/2})$ depends on an 'ideal' energy-level repartition

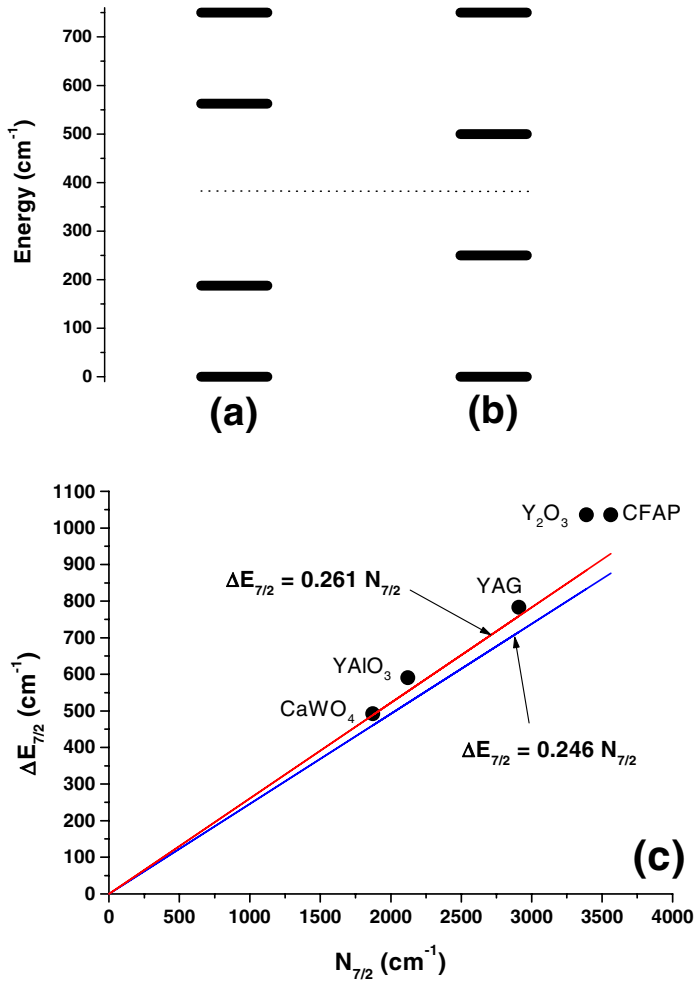

Figure 2. The idealized energy repartition of the $^2F_{7/2}$ manifold used in [19] (a) and in this work (b) to derive the dependence of the $^2F_{7/2}$ splitting on the crystal-field strength $N_{7/2}$ (c).

used to calculate this coefficient. The repartition used in [19] and leading to equations (2) and (4) is represented in figure 2(a). Using an equirepartition of the energy levels (figure 2(b)) leads to the following relation:

$$\Delta E(^2F_{7/2}) = 0.261 N(^2F_{7/2}). \tag{5}$$

The corresponding straight line is also represented in figure 2(c), and fits the experimental data better. At this stage, it seems possible to establish a simple relationship between $\Delta E(^2F_{7/2})$ and $\Delta E(^4I_{9/2})$. However, the N_J-parameter is not the same for neodymium and ytterbium ions in a given host: due to the lanthanide contraction, the sensitivity of these two ions to the crystal field is different. Nonetheless, a phenomenological study of this particular effect evidenced that there is a linear relation between these two crystal-field strengths [19]:

$$N(^2F_{7/2}) = 0.88 N(^4I_{9/2}). \tag{6}$$

Thus, by transitivity of the three linear relations $\Delta E(^4I_{9/2})$ proportional to $N(^4I_{9/2})$, $\Delta E(^2F_{7/2})$ proportional to $N(^2F_{7/2})$ and $N(^4I_{9/2})$ proportional to $N(^2F_{7/2})$, it appears that

the overall splitting of the ytterbium ground state in a given host is proportional to the one obtained for the Nd^{3+} $^4I_{9/2}$ manifold in the same host. More precisely, taking into account equation (5), this relation is [19]

$$\Delta E(^2F_{7/2}) \approx 1.6\,\Delta E(^4I_{9/2}). \tag{7}$$

In contrast to Yb-activated materials, Nd-doped compounds have been extensively studied [20]. The systematic use of equation (7) should then be an efficient way to detect new attractive hosts for Yb doping. This result is also useful for determining energy-level distributions from low-temperature spectroscopic data, as will be shown in sections 3.3 to 3.8 of the paper.

3. Low-temperature spectroscopy of new Yb-doped laser materials: determination of the energy levels

3.1. Spectroscopic requirements and selection of the compounds

As mentioned above, it is rather difficult to predict crystal-field interaction effects. Therefore, our strategy for obtaining high crystal-field strengths was to find compounds providing distorted host sites, characterized by a low point symmetry and a large distribution of Yb–O distances. Such characteristics occur for almost all the compounds selected here, as shown in table 2. In this respect, the most remarkable host matrices are the three silicate hosts, as well as the $Ca_3RE_2(BO_3)_4$ (RE = Y, Gd) double borates. RE^{3+} ions are highly coordinated, with mean RE–O distances of about 2.3–2.4 Å, and one to three oxygens situated at longer distances than the others. This peculiar arrangement is thus very distorted, which is expected to provide a large crystal-field splitting of the Yb^{3+} manifolds. In the case of $M_3RE(BO_3)_3$ (M = Ba, Sr and RE = Lu, Y) compounds, the sites are more regular, but characterized by particularly short RE–O distances, which should be favourable for creating a strong local crystal-field strength.

Table 2. Host sites of the different matrices.

Host	Space group	Host sites			$RE–O_{min}$ (Å)	$RE–O_{max}$ (Å)
		Label	Symmetry	Coordination		
$Ca_3Y_2(BO_3)_4$ (CYB)	$Pc2_1n$		C_1	8	2.35	2.69
			C_1	7 + 1	2.23	2.93
$Ba_3Lu(BO_3)_3$ (BLuB)	$P6_3cm$	Site Lu1	C_3	6	2.08	2.20
		Site Lu2	C_{3v}	6	2.12	2.20
$Sr_3Y(BO_3)_3$ (SrYBO)	$R\bar{3}$	Site 1	S_6	6	2.13	2.13
		Site 2	S_6	6	2.19	2.19
Y_2SiO_5 (YSO)	$C2/c$	Site 1	C_1	6 + 1	2.19	2.66
		Site 2	C_1	6	2.18	2.30
$Ca_2Al_2SiO_7$ (CAS)	$P\bar{4}2_1m$		C_1	6 + 2	2.43	2.86
$SrY_4(SiO_4)_3O$ (SYS)	$P6_3/m$	Site 6h	C_s	7	2.24	2.68
			C_3	6 + 3	2.38	2.79

A second criterion for selecting such materials concerns the broadness of the transition lines. Broad absorption lines are necessary to increase diode pumping efficiency, because laser diodes typically emit in a 5 nm wide spectral range, and present a thermal shift of the peak wavelength. On the other hand, broad emission lines are desirable for observing a tunable laser effect and generating ultrashort pulses. To obtain wide absorption and emission lines, the

selected materials must combine structural disorder and a multisite character [21]. However desirable for diode-pumped laser operation, this broadness of the transition lines increases the difficulty of deriving ytterbium energy-level diagrams from the low-temperature spectra.

All the crystals studied here were Czochralski grown, as described elsewhere [21]. A detailed study of both low-temperature absorption and emission properties of each Yb-doped sample was performed. The crystals, tailored for laser applications, were heavily doped, which prevents a rigorous spectroscopic study. In some cases, diluted samples were also prepared. As will be shown below, the only difference observed then concerned the zero line (associated with the transition between the $^2F_{7/2}$ and $^2F_{5/2}$ lowest Kramers doublets), which was weaker for the highly doped crystals in emission spectra, due to marked reabsorption processes.

3.2. Experimental procedure

The unpolarized absorption spectra were recorded on a Varian Cary 5E double-beam spectrophotometer. The unpolarized emission spectra were measured using a Ti:sapphire laser beam excitation (Coherent 890, 1 W output power, excitation wavelength in the range 900–950 nm). The emitted light was collected through a 0.75 m grating monochromator, the detector being a PbS cell. During all of the experiments, the crystals were cooled down using an Oxford Instrument cryogenerator. The working temperature was about 15 K during absorption measurements, whereas it reached 50 K under laser beam irradiation for emission measurements.

In each case, the absorption and emission spectra were adjusted to the same energy scales, the origin being taken at the lowest-energy absorption line. On this scale, vibronic lines associated with a given phonon and related to the zero-line transition should occur at the same energy in emission and absorption. Therefore, transition lines which are superimposed across the two spectra are likely to correspond to vibronic transitions.

3.3. Yb:$SrY_4(SiO_4)_3O$

The low-temperature absorption and emission spectra of a 6 at.% Yb-doped SYS crystal are presented in figure 3. In order to illustrate the following discussion, a rough decomposition of the spectra using Lorentzian lines is also presented. Superimposed lines (dotted curves), which are likely to correspond to vibronic transitions, are linked by vertical dotted lines whereas the remaining intense lines (continuous curves), which could be attributed to electronic transitions, are labelled by letters. It is noticeable that even at low temperature, these lines remain broad and somewhat unresolved. This is due to structural disorder in this lattice, in which strontium and yttrium equally share the same type of Wyckoff site, namely 4f sites. The second host site of the structure is 6h; sites of this type are exclusively occupied by yttrium. A statistical substitution of Yb^{3+} for Y^{3+} ions is expected over the 4f and 6h sites, due to the similarity of their ionic radii. In this case, the doping ions mostly lie at the 6h sites, in a population ratio of 3/1. Therefore, the intense lines in the spectra are likely to correspond to electronic levels of ytterbium ions lying at the 6h sites.

Among the intense lines labelled by letters, A and A′ superimpose well at this energy scale. This could indicate that they are vibronic lines. However, they are strong enough to be also considered as potential electronic lines. At this stage there remain, in addition to the zero line, four emission and three absorption lines. In each spectrum, one of these lines does not correspond to an electronic transition. In order to determine which of them correspond to electronic transitions, the following procedure is used. The six possible energy-level diagrams are built (figure 4(a)), and their representative points reported in the barycentres

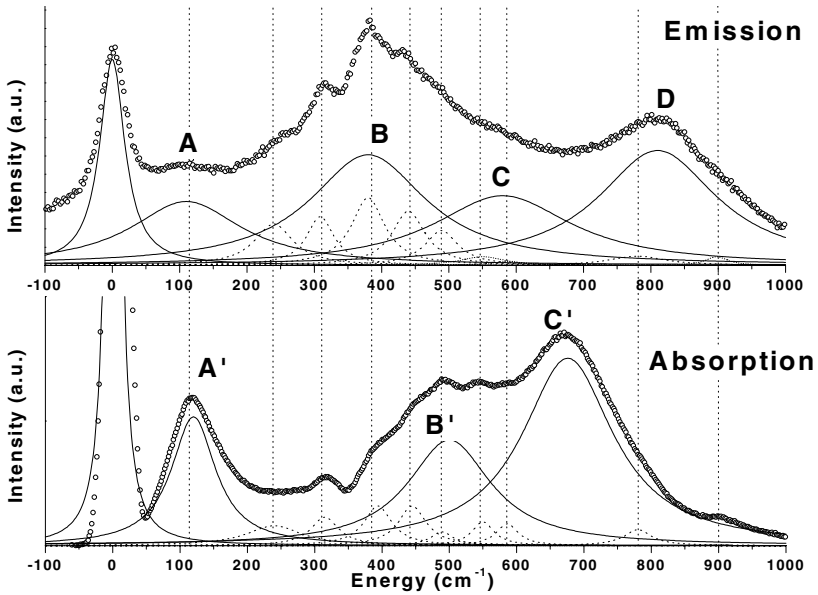

Figure 3. Low-temperature absorption and emission spectra for 6 at.% doped Yb:SYS.

plot (figure 4(b)). The points closest to the straight line correspond to energy-level diagrams D1 and D6. To choose between these two configurations, other arguments have to be considered. Firstly, diagram D1 involves lines A and A′, which may also be assigned as vibronic lines. Secondly, the SYS host is an oxyapatite, structurally similar to the fluorapatites CFAP, SFAP and SVAP. It is thus reasonable to consider that the SYS representative point in the barycentres plot should be close to the points associated with the fluorapatites. The two arguments converge, and D6 is probably the Yb^{3+} energy-level diagram for the 6h sites of Yb:SYS.

3.4. Yb:$Ca_2Al_2SiO_7$

This compound presents a high degree of structural disorder. As for the Yb:SYS material, this is due to the fact that aluminium and silicon ions share one type of tetrahedral site. This disorder is enhanced in the case of Yb-doped crystals, as the doping ion charge has to be compensated since ytterbium ions lie at the Ca^{2+} sites [22]. Therefore, low-temperature absorption and emission lines are poorly resolved (figure 5). However, a similar procedure to that used for Yb:SYS leads to consistent ytterbium energy levels in this host. Their energies are reported in table 3, along with results concerning all the compounds studied here. The corresponding point in the barycentres plot is represented in figure 13—see later.

3.5. Yb:Y_2SiO_5

The low-temperature absorption and emission spectra are presented in figure 6. The major lines are marked by letters (except for C′, which labels the group of lines around 200–400 cm^{-1} in the absorption spectrum). A striking feature of both spectra is the splitting of the zero line into two peaks, which are narrower than all the other major lines. This splitting could result from a reabsorption–emission process. In order to investigate this possibility, a weakly doped powder

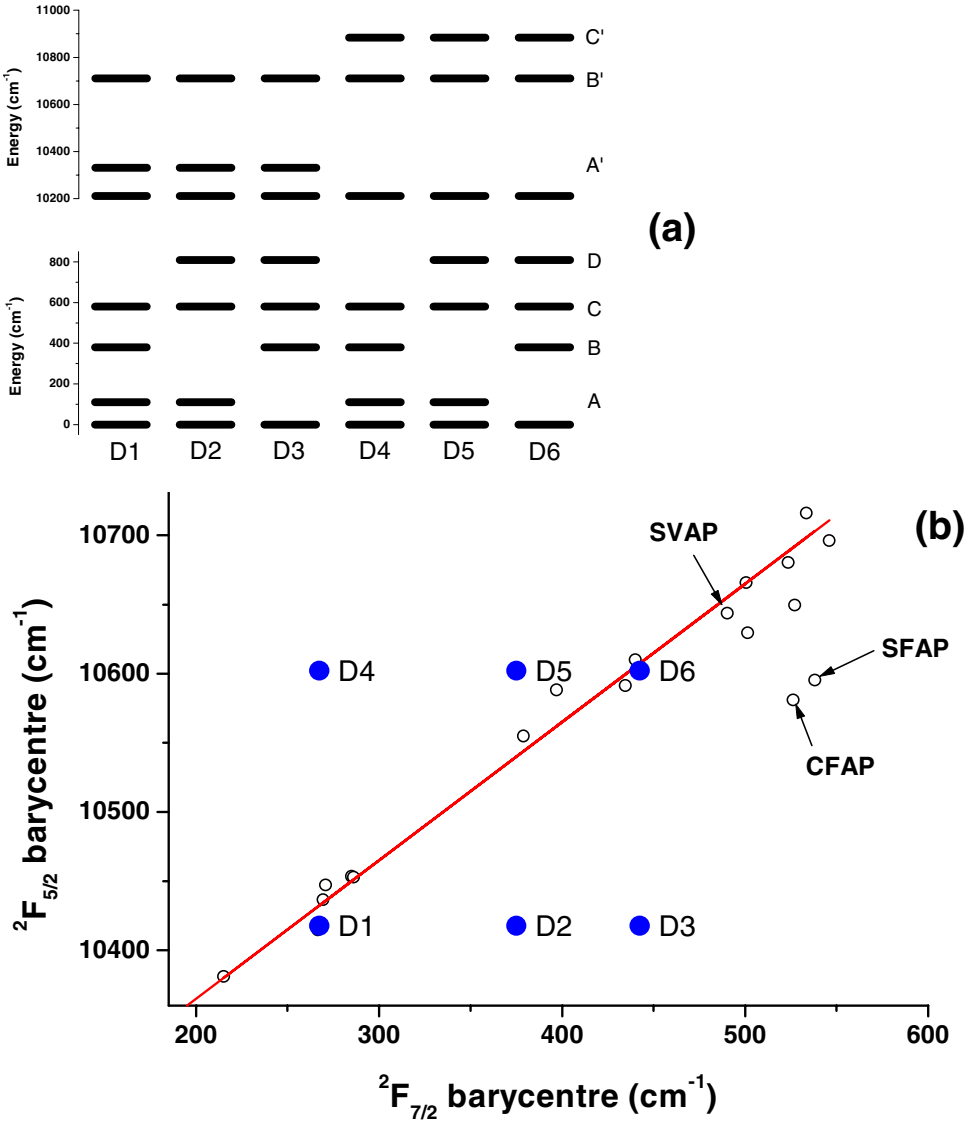

Figure 4. Possible energy-level diagrams for Yb^{3+} in SYS (a) and corresponding points in the barycentres plot (b).

sample (0.5 at.%) was synthesized, and its fluorescence spectrum recorded at low temperature. This spectrum is plotted in figure 7(a), along with the emission spectrum of the 5 at.% doped crystal. It can be seen that the splitting of the zero line still persists at this low doping level, where reabsorption–emission phenomena should be much weaker. In fact, as mentioned in the experimental section, a reabsorption process occurs in the case of the highly doped sample, but mainly results in a weaker intensity of the A and B zero lines in comparison with the other lines of the spectrum. This leads us to conclude that this splitting corresponds to the separate contributions of the two populations of doping ions at the two distinct yttrium crystallographic sites later on labelled site 1 and site 2 (see table 2).

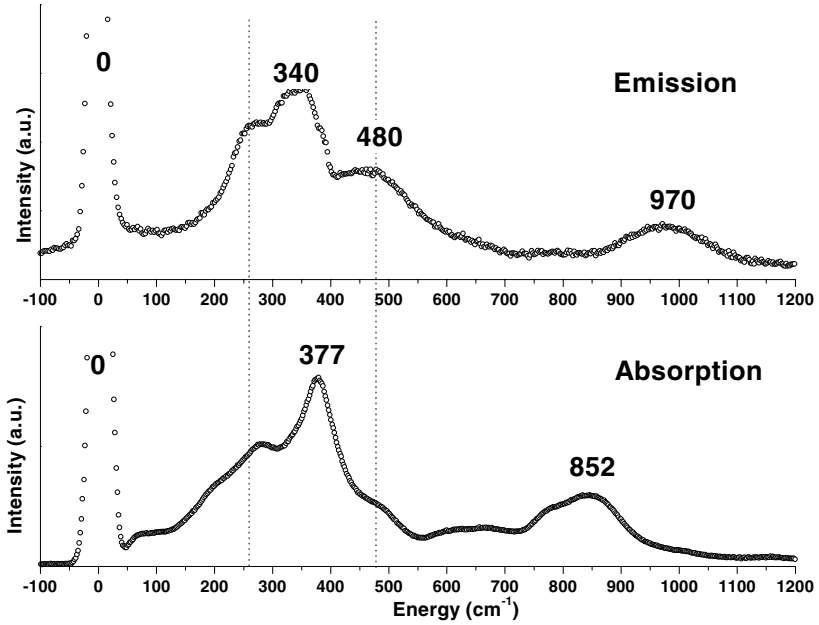

Figure 5. Low-temperature absorption and emission spectra for 0.5 at.% doped Yb:CAS.

Table 3. Ytterbium energy levels in the host matrices studied, as well as for Gd site in GdCOB [7].

Host	$^2F_{7/2}$ (cm^{-1})				$^2F_{7/2}$ barycentre (cm^{-1})	$^2F_{5/2}$ (cm^{-1})			$^2F_{5/2}$ barycentre (cm^{-1})
CYB	0			850	—	10250		10850	—
BLuB	0	408	428	900	434	10352	10377	11030	10589
SrYBO 1	0	274	614	859	437	10256	10475	11020	10584
SrYBO 2	0	179	469	734	346	10229	10405	10908	10514
SYS	0	380	580	810	443	10211	10711	10884	10602
CAS	0	340	480	970	448	10220	10600	11072	10631
YSO 1	0	113	494	715	331	10194	10420	10878	10497
YSO 2	0	236	615	964	454	10224	10517	11084	10611
GdCOB	0	423	668	1003	523.5	10246	10706	11089	10680

To go further into this analysis, let us compare the emission spectra of the 5 at.% and 0.5 at.% doped samples (figures 7(a) and 7(b)). If line A intensity is used as a reference, it is clear that line B is much more intense for the highly doped crystal. This can be explained by an Yb^{3+} population effect, as follows: at low concentration, the doping ions are distributed statistically over all possible sites in the structure, which lowers the crystal energy for entropic reasons. As the concentration increases, the site occupation becomes no longer statistical; the doping ions preferentially occupy the less energy-consuming sites: the entropy variation for each new Yb^{3+} ion added decreases and an enthalpic effect takes over. Therefore, the relative populations at the two sites could vary with the Yb^{3+} concentration, as observed here.

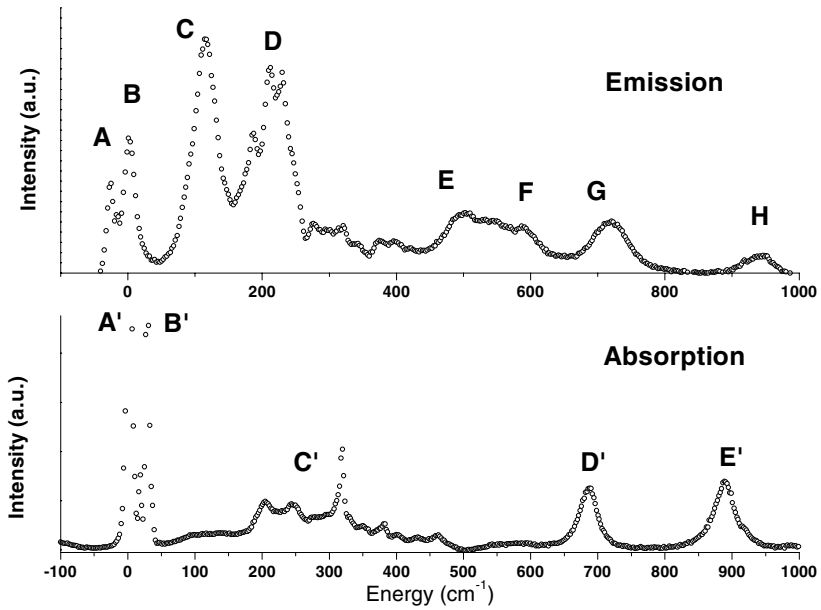

Figure 6. Low-temperature absorption and emission spectra for 5 at.% doped Yb:YSO.

This analysis can be extended to the other lines of the emission spectra, using line D as an intensity reference, as summed up in figure 7(b). It appears from this study that the lines C, E and G are slightly enhanced as the ytterbium concentration increases. Along with line B, they can be attributed to the contribution of one of the two host sites in the structure. This allows us to estimate a maximum splitting of 715 cm^{-1} for the $^2F_{7/2}$ manifold of Yb^{3+} at this site (site 1). Accordingly, the second contribution derived from the comparison of the two emission spectra corresponds to lines A, D, F and H, leading to a maximum splitting as high as 964 cm^{-1} (site 2). This splitting of the $^2F_{7/2}$ manifold is one of the largest known as far as Yb-doped compounds are concerned [2]. Ytterbium distribution over the two yttrium sites is not surprising, since such a distribution has already been reported for neodymium in Nd:YSO [23]. However, the Nd^{3+} ground-state splitting is given in [23] as being identical for the two sites (472 cm^{-1}). This result seems unlikely in view of the very different local surroundings of the two yttrium sites. Very different energy-level diagrams are also presented for Yb^{3+} in sesquioxide hosts where two different sites have been evidenced. According to the argument presented in section 2.2 of this paper, the 472 cm^{-1} splitting of the Nd^{3+} ground state is compatible with the 715 cm^{-1} splitting of the Yb^{3+} $^2F_{7/2}$ manifold at site 1, but not with the one observed at site 2.

Absorption spectra suggest assigning the D′ and E′ lines to the two different sites. It seems reasonable to assume that the site which gives the largest $^2F_{7/2}$ splitting is also the one with the largest $^2F_{5/2}$ splitting. Assuming that all of the lines considered up to now correspond to electronic transitions, only one energy level remains to be determined for each site, i.e. the intermediate Stark sublevel in the $^2F_{5/2}$ manifold. This can easily be done using the barycentres plot: both expected absorption lines are situated in the C′ group of lines, around 220 cm^{-1} and 300 cm^{-1} for sites 1 and 2 respectively. The energy levels for both sites as well as their representative points in the barycentres plot are reported in table 3 and figure 13, later.

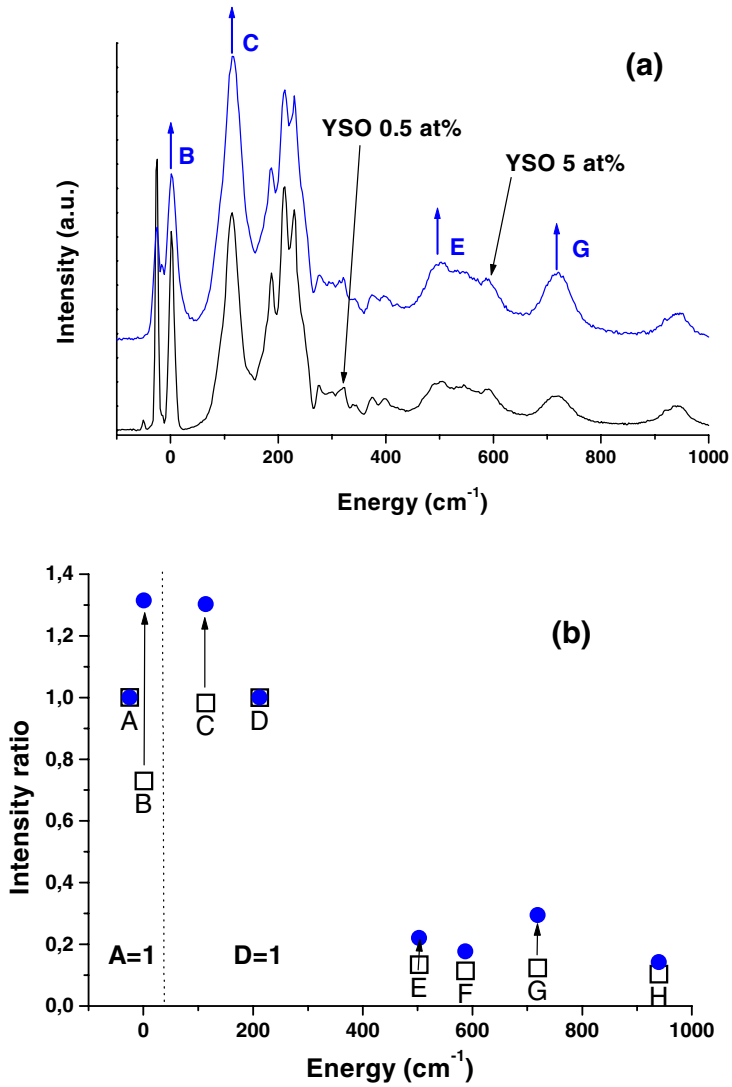

Figure 7. (a) Comparison of low-temperature emission spectra for 0.5 at.% and 5 at.% doped Yb:YSO (the latter being shifted for clarity). (b) Comparison of relative intensities for the different lines.

3.6. Yb:$Ba_3Lu(BO_3)_3$

Among the double borates studied here, Yb:BLuB presents the best-resolved low-temperature spectra (figure 8). The most remarkable feature concerning these spectra is the apparent splitting of the zero line into two components separated by about 25 cm^{-1}. This splitting could be explained by the presence of two distinct host sites in the lattice. However, the two crystallographic sites are very similar. Furthermore, several emission lines are split, whereas only the zero line in the absorption spectrum is split, by 25 cm^{-1}. In fact, there is only one intense absorption line at 678 cm^{-1} which is likely to correspond to an electronic transition. The absence of different sites could be confirmed by the characterization of a diluted

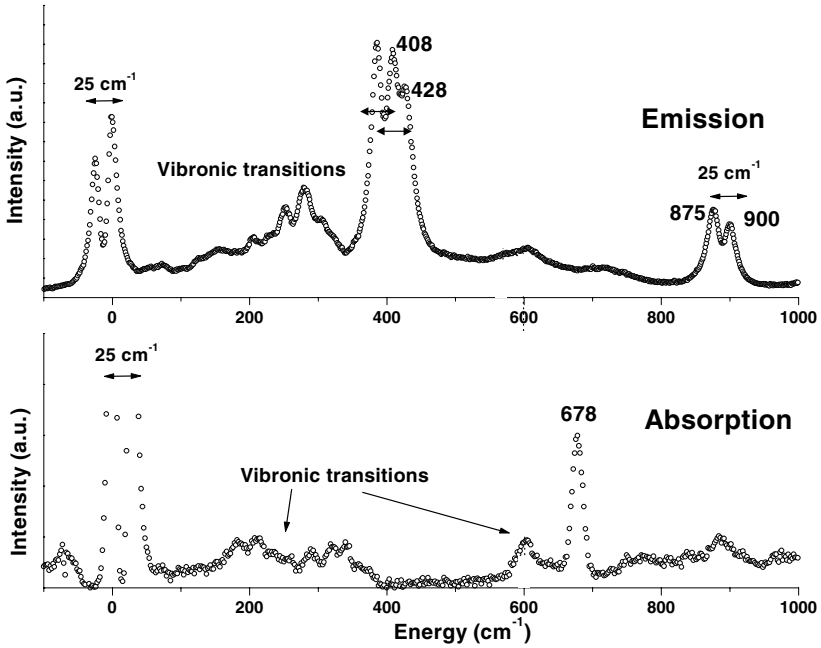

Figure 8. Low-temperature absorption and emission spectra for 15 at.% doped Yb:BLuB.

sample. However, due to the weak absorption and emission cross-sections of Yb:BLuB, the interpretation of the spectra recorded for a diluted sample would be difficult because of the poor signal-to-noise ratio. It is also possible to consider a reabsorption–emission process to explain the zero-line splitting; however, such a phenomenon cannot account for the constant splitting of the other emission lines.

This particular configuration of the spectra suggests the following interpretation. The $^2F_{5/2}$ excited-state sublevels at the two sites are probably non-uniformly distributed, with the two lower sublevels very close to each other, only separated by 25 cm^{-1} (figure 9). Three intense lines in the absorption spectrum reflect this distribution. Owing to this peculiar arrangement, the $^2F_{5/2}$ second Stark sublevel would be thermally populated during the emission measurement at about 50 K. This sublevel could then contribute to the fluorescence. The two contributions would be identical, only shifted from 25 cm^{-1}, as observed in the emission spectrum. Another argument corroborates this interpretation, as the zero-line transition occurs in the case of Yb:BLuB at 966 nm, which is a particularly short wavelength in comparison with those for other Yb-doped materials [2]. This is easily explained by the peculiar arrangement of the $^2F_{5/2}$ sublevels: the two lower levels are closer to the $^2F_{5/2}$ barycentre than in the case of an equirepartition (figure 9). Hence, the $^2F_{5/2}$ lowest Stark level is situated at higher energy.

3.7. Yb:$Sr_3Y(BO_3)_3$

In the case of Yb:SrYBO, which also offers two distinct yttrium sites, the transition lines are broad and poorly resolved, and of similar intensities (figure 10). Among them, the absorption line situated around 950 cm^{-1} is probably due to a vibronic transition. Stretching vibrations of the BO_3^{3-} anions are expected to occur in this energy range, like in the $Ca_4GdO(BO_3)_3$ (GdCOB) material [7]. Furthermore, the overall splitting of the excited $^2F_{5/2}$ manifold is not

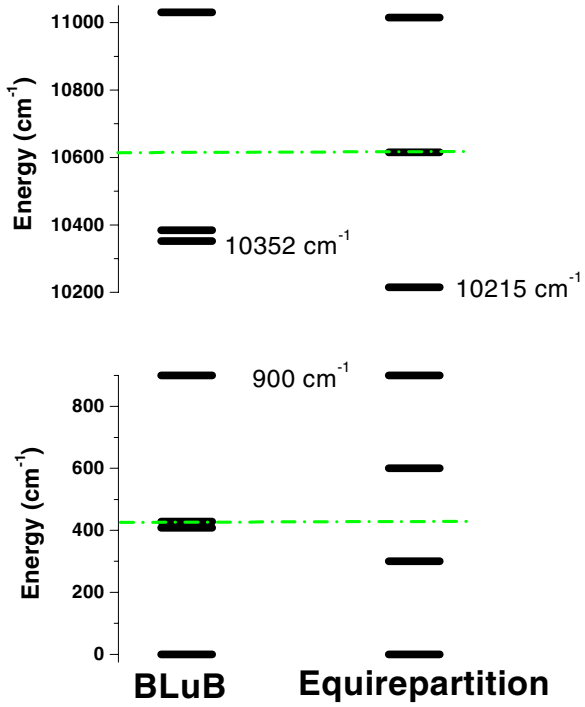

Figure 9. The energy-level distribution of ytterbium in BLuB in comparison with an equirepartition of the electronic levels.

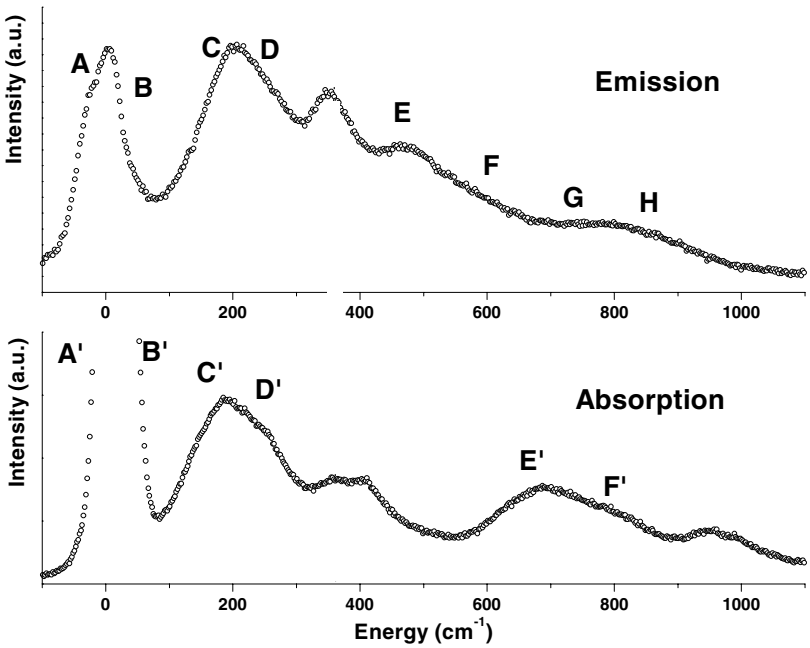

Figure 10. Low-temperature absorption and emission spectra for 15 at.% doped Yb:SrYBO.

likely to be larger than 850 cm^{-1}, which corresponds to the observed ground-state splitting. A second probable vibronic line is located around 360 cm^{-1} (good resonance in absorption and emission). All the remaining lines can correspond to electronic transitions. Moreover, a splitting of the zero line is also observed. Low-temperature absorption and emission spectra of weakly doped samples are shown in figure 11. In spite of the broadness of the transition lines, the two site contributions seem to be resolved in both spectra. As for the Yb:YSO compound, a comparison of the spectra obtained for the diluted and highly doped samples enables us to separate these two contributions. One can compare here both absorption and emission data, but due to the low doping level, the absorption and emission band intensities are weak, leading to a poor signal-to-noise ratio for the corresponding spectra. Therefore, the interpretation presents some uncertainties.

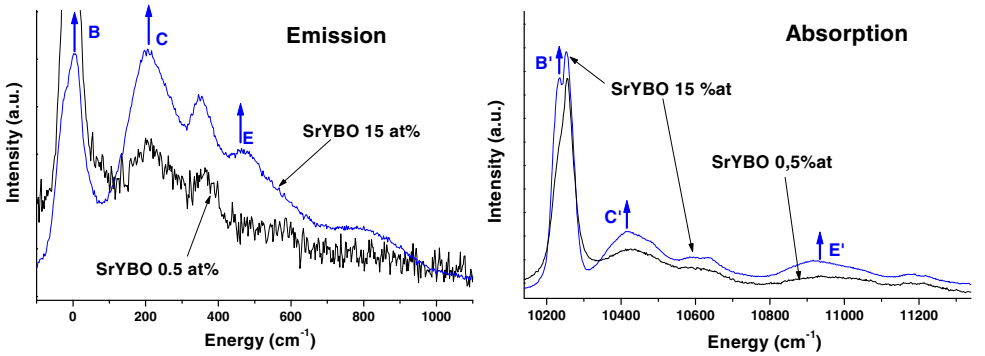

Figure 11. Comparison of low-temperature emission and absorption spectra for 0.5 at.% and 15 at.% doped Yb:SrYBO.

When comparing absorption and emission spectra of the two samples, it appears that lines B, C, E, B′, C′ and E′ are enhanced on increasing the dopant concentration. Hence, these lines could correspond to a first site. At this site, the only missing level is the highest $^2F_{7/2}$ sublevel, which also gives the total ground-state splitting. Considering the absorption spectrum, it appears that this contribution corresponds to the smallest $^2F_{5/2}$ splitting (given by the energy difference between B′ and E′). Accordingly, the $^2F_{7/2}$ splitting should correspond to the energy difference between B and G, the latter corresponding to the missing electronic level. With that attribution, the remaining lines (namely A, D, F, H, A′, D′ and F′) correspond to the second-site contribution. It is noticeable that in spite of the difficult analysis of the spectra for the weakly doped sample, this interpretation leads to energy-level diagrams which fit remarkably well in the barycentres plot, as shown in figure 13, later.

3.8. Yb:$Ca_3Y_2(BO_3)_4$ and Yb:$Ca_3Gd_2(BO_3)_4$

These two materials present very similar low-temperature absorption and emission spectra (see figure 12 for the Yb:CYB compound). These spectra are similar to absorption and emission ones obtained for Yb-doped glassy matrices. This is probably due to a particularly strong multisite character, as those hosts offer two RE^{3+} sites and three different calcium sites, which are also likely to be substituted with Yb^{3+} ions to some extent. For the generation of ultrashort pulses, Yb:CYB and Yb:CaGB are very interesting, as they offer spectroscopic characteristics similar to those of Yb-doped glasses, with improved thermal properties due to their crystalline

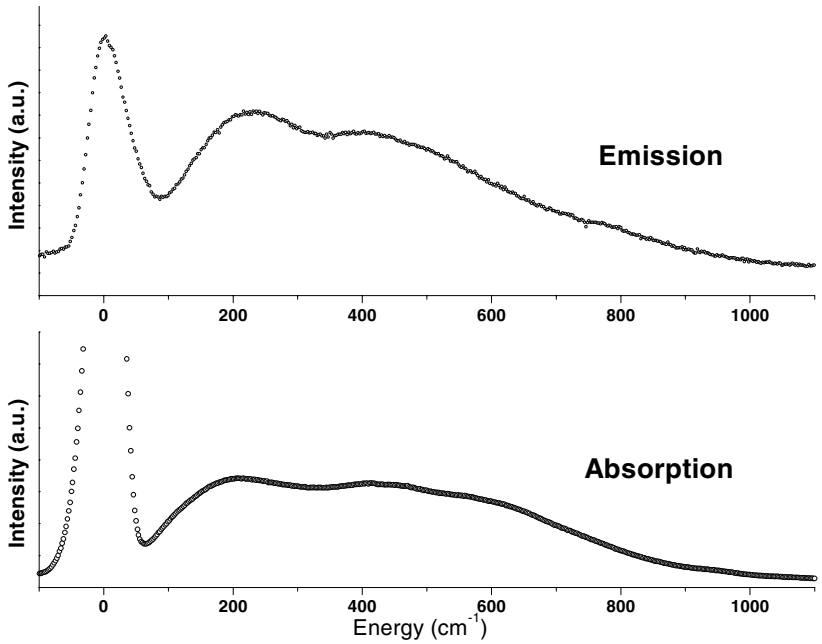

Figure 12. Low-temperature absorption and emission spectra of 10 at.% doped Yb:CYB.

structure. However, it is impossible to derive any energy-level diagram from such unresolved spectra. It is only possible to estimate the maximum splitting of the ytterbium manifolds. It appears that ytterbium experiences quite a strong crystal-field interaction, as the $^2F_{7/2}$ splitting reaches about 850 cm^{-1} in these two hosts.

3.9. Summary

All the results derived from the analysis of low-temperature spectra for all the compounds considered are gathered in table 3. As expected, the ytterbium ions experienced a strong crystal-field interaction in each of these materials, leading to a large overall splitting of the Yb^{3+} ground state. This splitting always exceeds 800 cm^{-1}, and reaches 970 cm^{-1} in the case of Yb:CAS. However, although consistent with the barycentres plot (figure 13), the given interpretation is in most cases somewhat tentative, and still needs to be confirmed. This is the purpose of the next section of this paper.

4. The point charge electrostatic crystal-field model: a predictive tool for the Yb^{3+} hosts?

The purpose of this section is twofold. On one hand, we propose to use the point charge electrostatic crystal-field model (PCEM) in a simple way as a predictive tool to determine the crystal-field potential experienced by Yb^{3+} ions in a given host from crystallographic and structural data only. At the same time, the validation of this procedure in the case of the silicate and borate hosts studied in this paper will confirm the energy-level diagrams deduced from the low-temperature spectroscopic data.

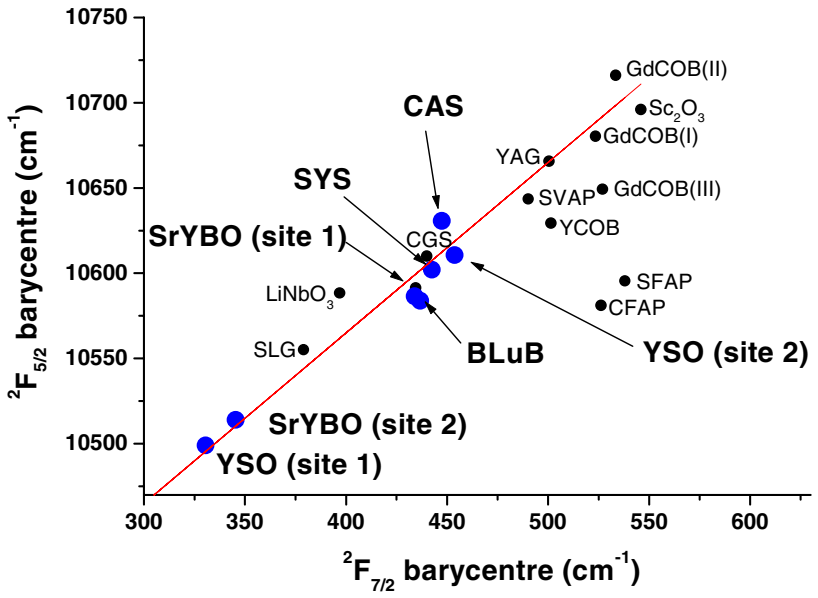

Figure 13. Representation of the Yb-doped materials studied in a barycentres plot.

According to this PCEM [3], the electrostatic potential created at the site considered (position r_0) by the N constitutive ions (position r_n, charge q_n) of the crystal is given by

$$U(r_0) = \sum_{k=0}^{\infty} \sum_{q=-k}^{k} \left[\frac{1}{4\pi\varepsilon_0} \sum_{n=1}^{N} \frac{q_n}{r_n^{k+1}} (-1)^q C_{k-q}(\theta_n, \varphi_n) \right] r_0^k C_{kq}(\theta_0, \varphi_0)$$
$$U(r_0) = \sum_{k=0}^{\infty} \sum_{q=-k}^{k} A_{kq} r_0^k C_{kq}(\theta_0, \varphi_0). \tag{8}$$

Equation (8) indicates that the A_{kq}-parameters, which characterize the crystal-field potential, are thus determined by a lattice-sum calculation from structural data. In the following calculations, ytterbium ions were assumed to enter the hosts without modifying the atomic coordinates. This is quite reasonable in the case of yttrium-based compounds, as ytterbium and yttrium present similar ionic radii. In order to obtain convergence in all cases, constitutive ions situated in a sphere of radius $R = 130$ Å around the site studied were considered.

In order to obtain realistic results, several improvements have to be made. The first one consists in modifying the radial integrals as follows [3]:

$$\langle r^k \rangle_{eff} = \frac{\langle r^k \rangle}{\tau^k} (1 - \sigma_k) \tag{9}$$

where τ is a coefficient which accounts for a spreading of the 4f wave functions when the doping ion is embedded in a crystal ($\tau = 0.6532$ [24]), and the σ_k-parameters correspond to the Sternheimer screening. The values of those coefficients used here are given in table 4. The second way to improve the results consists in taking into account the covalency of the solid. This is done by using effective charges for the constitutive ions instead of their formal ionic charge. For instance, an effective charge of the oxygen ions equal to $-1.8e$ has been used to calculate crystal-field parameters for CFAP [12]. Hence, these effective charges are the adjustable parameters of the model.

Table 4. Screening coefficients and effective radial integrals used in this study [24].

	σ_k	$\langle r^k \rangle_{eff}$
$k = 2$	0.5683	0.6599
$k = 4$	0.0472	5.9037
$k = 6$	−0.0406	52.677

This model was used to calculate crystal-field parameters for four of the compounds studied, namely YSO, SYS, SrYBO and BLuB. In order to complete this study, GdCOB [7] and $YAl_3(BO_3)_4$ (YAB) [9] were considered as well. All of these materials can be divided into two groups: silicates on one hand, BO_3-based borates on the other hand. The PCEM program used in this work (developed by Dr P Porcher [25]) allows us to perform crystal-field calculations at arbitrary r_0-positions in the unit cell. This enabled us to determine the crystal-field parameters for different host sites whenever needed, just by changing this origin. In each case, the crystal-field potential deduced was used to derive an energy-level diagram for ytterbium, using the SPECTRA program developed at Argonne National Laboratory [26]. In order to adjust experimental and calculated energy levels by varying effective charges, no automatic refinement was carried out; instead, a simultaneous study of the various hosts was undertaken. The purpose was to keep the effective charges very similar for the different materials in each of the two families.

This approach led to particularly consistent results, as shown in figure 14. For all compounds studied, the match between calculated and experimental energy-level diagrams is striking. In most cases, this model led not only to a correct estimation of the ytterbium manifolds' overall splitting—which was the main purpose of this work —but also confirmed the repartition of the intermediate Stark sublevels. This is particularly spectacular in the case of YSO and SrYBO, where the energy-level diagrams for both sites are obviously confirmed. It is noticeable from these results that YSO presents two very different sites. In contrast,

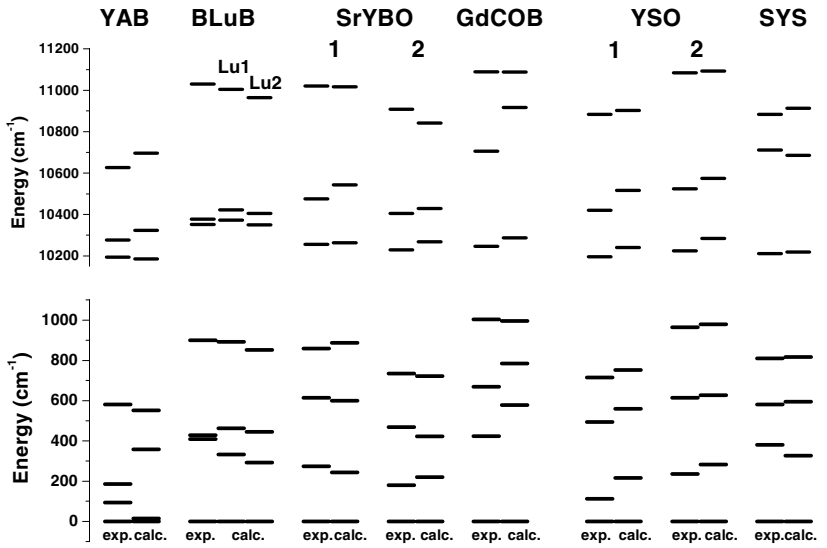

Figure 14. Experimental and calculated energy-level diagrams for ytterbium in various borate and silicate hosts.

calculations performed for the two lutetium sites in the BLuB structure lead to similar results, both close to the observed energy-level distribution. This explains why the two contributions were not separated in the low-temperature absorption and emission spectra.

The effective charges deduced from this approach are gathered in table 5, evidencing that the energy levels described above were obtained with almost constant effective charges of oxygen and boron or silicon through the borate and silicate host series respectively. This means that SiO_4^{4-} tetrahedra and BO_3^{3-} triangles show very little environment dependence. This is of extreme importance, as it evidences that the PCEM can be used as a predictive tool, using the same effective charges in the case of new silicates or BO_3-based borates. It is also noticeable that the oxygen effective charge is larger for Si–O ($-0.85e$) than for the B–O bonds ($-0.5e$). This is in good agreement with the fact that B–O bonds are expected to be more covalent than Si–O bonds, on the basis of the electronegativity difference (1.7 for Si–O versus 1.5 for B–O). Accordingly, oxygens which do not belong to such structures (O′ in table 5) have more ionic effective charges: this is the case for SYS and GdCOB. Finally, in all cases, rare-earth ions present similar effective charges, around $1e$.

Table 5. Effective charges used for the different hosts in the PCEM.

Host	q_{RE}	q_{Si}	q_B	q_{Sr} or q_{Ca} or q_{Ba}	q_{Al}	q_O	$q_{O'}$
YSO	$1.2e$	$1.85e$				$-0.85e$	
SYS	$1.2e$	$2.0e$		$0.45e$		$-0.85e$	$-1.05e$
YAB	$0.9e$		$0.8e$		$0.63e$	$-0.5e$	
BLuB	$0.9e$		$0.83e$	$0.4e$		$-0.51e$	
SrYBO	$0.9e$		$0.8e$	$0.25e$		$-0.45e$	
GdCOB	$0.9e$		$0.8e$	$0.418e$		$-0.45e$	$-0.92e$

Hence, this approach appears to be attractive for determining the crystal-field splitting of ytterbium from just crystallographic data. However, this procedure should not be adopted in some cases. In particular, such calculations cannot be carried out for compounds where ytterbium doping introduces significant local changes in the structure. This is the case when the doping ion requires charge compensation, or when the host site is not well adapted to the doping ions in terms of size and must be distorted when there is substitution. Such effects occur for Yb:CAS, in which Yb^{3+} substitutes for Ca^{2+}. This is why PCEM calculations were not performed successfully in that case.

5. Conclusions

Laser performances of Yb-doped materials are strongly affected by the crystal-field interaction, as a large Yb^{3+} ground-state splitting is necessary to obtain a quasi-three-level laser operating scheme. Meanwhile, this crystal-field splitting is very different from one host to another and very difficult to predict.

One way is to synthesize the Yb^{3+}-doped compounds and to derive the ytterbium energy-level diagram from low-temperature optical spectra. However, from a practical point of view, attractive spectroscopic features for diode-pumping applications (broad absorption lines) as well as for tunable laser emission and ultrashort-pulse generation (broad emission lines) make the interpretation of low-temperature spectroscopic data difficult. Furthermore, interactions of ytterbium ions with the lattice vibrations complicate the spectra. In order to overcome these difficulties, a careful consideration of crystal-field effects combined with an exhaustive survey of available data concerning ytterbium provides useful tools. The first one is the ‘barycentres

plot', based on the fact that the spin–orbit splitting between $^2F_{7/2}$ and $^2F_{5/2}$ is host independent, and equal to the free-ion energy separation. The second tool is the linear relation linking the Yb^{3+} ($^2F_{7/2}$ level) and the Nd^{3+} ($^4I_{9/2}$ level) crystal-field splittings. Both approaches are useful for confirming or guiding the interpretation of the spectra, the latter also being an efficient tool for detecting new potentially attractive Yb-doped materials, as Nd doping has been extensively studied in laser materials.

These procedures were successfully applied to the new Yb-doped silicates Y_2SiO_5 (YSO), $Ca_2Al_2SiO_7$ (CAS) and $SrY_4(SiO_4)_3O$ (SYS) and borates $Ca_3Y_2(BO_3)_4$ (CYB), $Ca_3Gd_2(BO_3)_4$ (CaGB), $Sr_3Y(BO_3)_3$ (SrYBO) and $Ba_3Lu(BO_3)_3$ (BLuB). Despite the broad transition lines observed in these materials, energy-level diagrams have been derived in most cases. For YSO and SrYBO, contributions of two distinct crystallographic host sites were separated. As expected, it appears that in all the compounds studied, ytterbium manifolds are widely split: the $^2F_{7/2}$ overall splitting is always higher than 800 cm^{-1}, and reaches 970 cm^{-1} for Yb:CAS.

These experimental energy-level distributions found confirmation through PCEM crystal-field calculations. A simultaneous study of the compounds described above along with the $Ca_4GdO(BO_3)_3$ (GdCOB) and $YAl_3(BO_3)_4$ (YAB) matrices was carried out. All energy-level diagrams could be fitted using the same set of effective charges for the constituting ions through each of the two families (silicates and BO_3-based borates). This evidences that such calculations can be performed in a predictive approach, to determine the $^2F_{7/2}$ crystal-field splitting in new borates or silicates from just structural data. It is expected that this approach could be extended to other families, such as phosphates, vanadates or scheelite-like double tungstates.

Acknowledgments

The authors wish to thank DGA for financial support, Dr Porcher for the use of the PCEM program and for fruitful discussion, and B Ferrand (Leti-CENG) for the synthesis of the Yb:YSO samples. Dr F Auzel is also acknowledged for his great interest in this work.

References

[1] Stewen C, Larionov M, Giesen A and Contag K 2000 *OSA TOPS Adv. Solid-State Lasers* **34** 35
[2] de Loach L D, Payne S A, Chase L L, Smith L K, Kway W L and Krupke W F 1993 *IEEE J. Quantum Electron.* **29** 1179
[3] Morrison C A and Leavitt P 1982 *Handbook on the Physics and Chemistry of Rare Earths* (Amsterdam: Elsevier) ch 46
[4] Gruber J B, Zandi B and Merkle L 1998 *J. Appl. Phys.* **83** 1009
[5] Chang N C, Gruber J B, Leavitt R P and Morrison C A 1982 *J. Chem. Phys.* **76** 3877
[6] Ellens A, Andres H, Meijerink A and Blasse G 1997 *Phys. Rev.* B **55** 173
[7] Mougel F, Dardenne K, Aka G, Kahn-Harari A and Vivien D 1999 *J. Opt. Soc. Am.* B **16** 164
[8] Lupei A, Enaki V, Lupei V, Presura C and Petraru A 1998 *J. Alloys Compounds* **275–277** 196
[9] Wang P, Dawes J M, Dekker P, Knowles D S, Piper J A and Lu B 1998 *OSA TOPS Adv. Solid-State Lasers* **19** 565
[10] Kuleshov N V, Lagatsky A A, Podlipensky A V, Mikhailov V P and Huber G 1997 *Opt. Lett.* **22** 1317
[11] Becker P C, Hayhurst T, Shalimoff G, Conway J G, Edelstein N, Boatner L A and Abraham M M 1984 *J. Chem. Phys.* **81** 2872
[12] Morrison C A 1995 *Report* ARL-TR-708
[13] Gruber J B, Leavitt R P, Morrison C A and Chang N C 1985 *J. Chem. Phys.* **82** 5373
[14] Peters V, Mix E, Petermann K, Huber G and Noginov M A 2000 *CLEO Europe 2000 Technical Digest* p 387
[15] Malkin B Z, Leushin A M, Iskhakova A I, Heber J, Altwein M, Moller K, Fazlizhanov I I and Ulanov V A 2000 *Phys. Rev.* B **62** 7063

[16] Rukmini E, Renuka Devi A and Jayasankar C K 1994 *Physica* B **193** 166
[17] Antic-Fidancev E 2000 *J. Alloys Compounds* **300+301** 2
[18] Auzel F and Malta O L 1983 *J. Physique* **44** 201
[19] Auzel F 2000 *Proc. 2nd Int. Symp. on Laser, Scintillator and Nonlinear Optical Materials (Lyon, 28–31 May 2000)* at press
[20] Kaminskii A A 1996 *Crystalline Lasers: Physical Processes and Operating Schemes* (Boca Raton, FL: Chemical Rubber Company Press) chs 2, 3
[21] Haumesser P-H, Gaumé R, Benitez J-M, Viana B, Ferrand B, Aka G P and Vivien D 2001 *J. Cryst. Growth* at press
[22] Lejus A M, Kahn-Harari A, Benitez J M and Viana B 1994 *Mater. Res. Bull.* **29** 725
[23] Tkachuk A M, Przhevusskii A K, Morozova L G, Poletimova A V, Petrov M V and Korovkin A M 1986 *Opt. Spectrosk.* **60** 176
[24] Morrison C A 1982 Lectures on crystal field theory *Report* HDL-SR-82-8
[25] Hälsä J and Porcher P 1990 Somaille software
[26] http://chemistry.anl.gov/spectra
[27] Simondi-Teisseire B 1996 *PhD Thesis* Paris VI University
[28] Mougel F 1999 *PhD Thesis* Paris VI University
[29] Gruber J B, Zandi B and Merkle L 1998 *J. Appl. Phys.* **83** 1009
[30] Bogomolova G A, Bumagina L A, Kaminskii A A and Malkin B Z 1977 *Sov. Phys.–Solid State* **19** 1428
[31] Wang P, Dawes J M, Dekker P, Knowles D S, Piper J A and Lu B 1999 *J. Opt. Soc. Am.* B **16** 63
[32] Mix E 1999 *PhD Thesis* Hamburg University
[33] Payne S A, DeLoach L D, Smith L K, Kway W L, Tassano J B and Krupke W F 1994 *J. Appl. Phys.* **76** 497
[34] Schaffers K I, DeLoach L D and Payne S A 1996 *IEEE J. Quantum Electron.* **32** 741
[35] Montoya E, Sanz-Garcia J A, Capmany J, Bausa L E, Diening A, Kellner T and Huber G 2000 *J. Appl. Phys.* **87** 4056